JTTEE5 15:725-730
DOI: 10.1361/105996306X146839
1059-9630/$19.00 © ASM International

Effect of Substrate Roughness on Splatting Behavior of HVOF Sprayed Polymer Particles: Modeling and Experiments

M. Ivosevic, V. Gupta, J.A. Baldoni, R.A. Cairncross, T.E. Twardowski, and R. Knight

(Submitted February 24, 2006; in revised form April 14, 2006)

A three-dimensional model of particle splatting on rough surfaces has been developed for high-velocity oxyfuel (HVOF) sprayed polymer particles and related to experimentally observed polymer splats. Fluid flow and particle deformation were predicted using a volume of fluid (VoF) method using Flow-3D software. Splatting behavior and final splat shapes were simulated on a realistic rough surface, generated by optical interferometry of an actual grit-blasted steel surface. Predicted splat shapes were compared with scanning electron microscopy images of nylon 11 splats deposited onto grit-blasted steel substrates. Rough substrates led to the formation of fingers and other asymmetric three-dimensional instabilities that are seldom observed in simulations of polymer splatting on smooth substrates.

Keywords HVOF spraying of polymers, polymer splats, surface roughness

1. Introduction

Substrate roughness enhances the adhesion of thermally sprayed coatings (Ref 1). Before spraying, substrate surfaces are typically roughened by grit blasting using 50 to 300 μm angular ceramic particles such as Al_2O_3 or SiC. The morphology of the initial splats deposited onto a substrate surface plays an important role in the overall integrity of the coating/substrate interface and the resulting adhesive and cohesive strength of the coating. The impact and deformation of thermally sprayed droplets onto a rigid, irregular surface are characterized by complex large-scale three-dimensional (3D) deformation of the droplet surfaces. In cases where "splashing" of the impacting droplets occurs, the creation of new surfaces during fingering and/or the generation of satellite particles and breakup is typically not axisymmetric, which would require a 3-D model for realistic splat predictions. This presents a number of numerical challenges for the development of an accurate 3-D splatting model. Fauchais et al. (Ref 2) reported that the majority (~98%) of published papers discussing splat formation processes described normal droplet impact onto smooth surfaces. Less than 2% of published work relates to nonnormal particle impacts on smooth surfaces, and only ~0.1% relates to rough substrates. Several authors (Ref 3, 4) have studied the interactions of a droplet with nonsmooth surfaces using two-dimensional (2D) models or 3D impacts on surfaces with parallel groves (Ref 5); however, the main disadvantage of this approach is the inability to study the nonaxisymmetric aspects of splatting on a rough surface. Fukanuma (Ref 6) studied the extent of droplet spreading on 3D prototypical surfaces consisting of regularly ordered cones, pyramids, and cylinders and concluded that spreading time and ratio decreased with increases in nominal surface roughness. Recently, Raessi et al. (Ref 7) also extended a previously developed volume of fluid (VoF) model (Ref 8) of droplet splatting on flat substrates to droplet interaction with a prototypical rough surface. The surface roughness was approximated by regularly ordered square blocks. Feng et al. (Ref 9) used a three-dimensional Lagrangian finite-element model where the surface roughness was approximated by a frictional condition on a flat surface. Although this approach can be accurate with respect to small-scale viscous and axisymmetric free surface flows, droplet splashing involving the creation of new surfaces during fingering and/or generation of satellites and breakups are not amenable to boundary-fitted techniques. Moreover, the average surface roughness (R_a) of a grit-blasted surface used in thermal spray is typically ~5 to 30% (~2 to 15 μm) relative to a mean droplet size of 50 μm, which may be too large to be approximated by simple frictional flow on a flat surface.

2. Objective

The primary objective of this work was to develop a 3D model of the splatting of high-velocity oxyfuel (HVOF) sprayed polymer particles impacting onto an arbitrary rough substrate. A particle splatting model on nonsmooth surfaces would provide an improved understanding of how the geometrical irregularities of a surface affect the splatting behavior and final polymer splat morphology.

This article was originally published in *Building on 100 Years of Success, Proceedings of the 2006 International Thermal Spray Conference* (Seattle, WA), May 15-18, 2006, B.R. Marple, M.M. Hyland, Y.-Ch. Lau, R.S. Lima, and J. Voyer, Ed., ASM International, Materials Park, OH, 2006.

M. Ivosevic, V. Gupta, R. Knight, and **R.A. Cairncross,** Drexel University, Philadelphia, PA; **J.A. Baldoni,** Duke University, Durham, NC; and **T.E. Twardowski,** Widener University, Philadelphia, PA. Contact e-mail: mi25@drexel.edu.

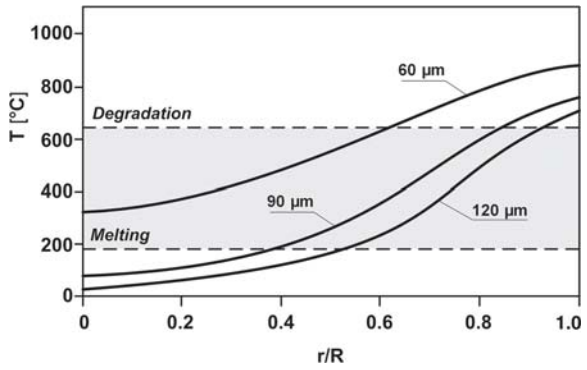

Fig. 1 Temperature of a 90 µm diameter nylon 11 particle with respect to normalized particle radius (r/R) (Ref 10).

3. Background

Forced convection from an HVOF jet to a micron-sized feedstock particle is characterized by a high convective heat transfer coefficient [$h \cong 5000$ to 17,000 W/(m^{2}K)]. This results in a rapid increase in particle surface temperature; however, the high internal thermal resistance [high Biot (Bi) number > 5] of polymer particles relative to metal particles (Bi < 0.1) prevents the interior of the particle from being heated at the same rate. Consequently, larger particles (>50 µm in diameter) develop a steep temperature gradient between the core and surface (Fig. 1) under the selected HVOF condition (Ref 10, 11). For example, a 90 µm diameter particle has a core region (<36 µm: $r/R = 0.4$) below the melting temperature of nylon 11 (182 to 191 °C), while the surface region (>77 µm: $r/R = 0.85$) has a temperature exceeding the upper degradation limit of the polymer (560 °C). Similarly, a 120 µm diameter particle was predicted to have an unmelted core and surface temperature above the degradation temperature, whereas a 60 µm diameter particle was predicted to be fully melted and to have almost 50% of its volume above the degradation temperature.

It was previously reported (Ref 11, 12) that HVOF sprayed nylon 11 particles with steep internal temperature gradients spread into a characteristic "fried-egg" shape with a large, nearly hemispherical, core in the center of a thin disk (Fig. 2). This shape indicated the existence of a large radial difference between the flow properties of the low-temperature, high-viscosity core and the high-temperature, low-viscosity surface. The predicted shapes of deformed particles (Fig. 2a) exhibited good qualitative agreement with experimentally observed splats deposited onto a glass slide (Fig. 2b). The velocity field vectors shown on the right-hand side of the droplet (Fig. 2a) indicated that the characteristic "fried-egg" splat shape was formed as the low-viscosity "skin" flowed around a high viscosity core.

The HVOF spray parameters used during the experiments reported here represent typical HVOF spray parameters used to deposit nylon 11. A numerical model developed around the experimental baseline parameters, however, can be used to better understand the flow behavior of individual splats and assist in process optimization for increased deposition efficiency.

The previously developed approach for the spreading of the HVOF sprayed nylon 11 particles on a flat substrate (Ref 11, 13) has been used here to further study the interaction of individual splats with an arbitrary rough substrate.

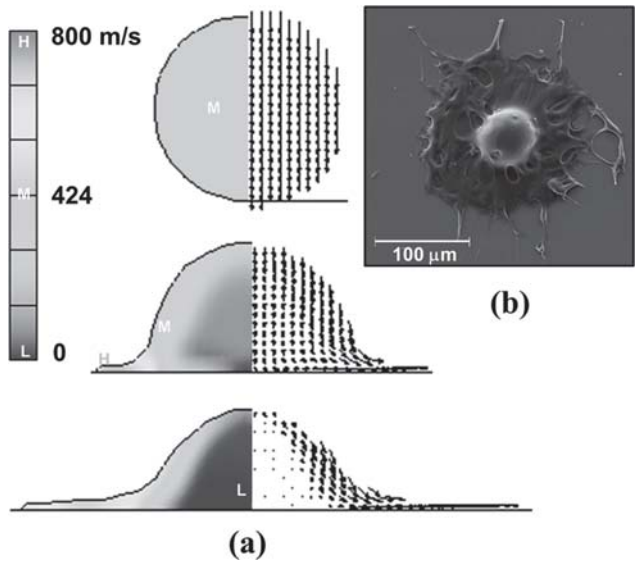

Fig. 2 (a) Velocity field within a spreading 90 µm diameter particle: left, velocity magnitude; right, velocity vectors. (b) Example of a nylon 11 splat deposited via swipe test onto a room-temperature glass slide

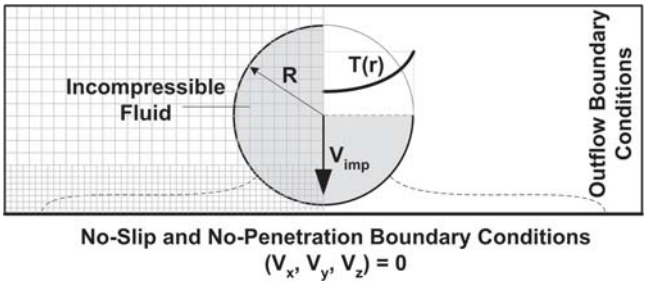

Fig. 3 Boundary conditions, initial conditions, and cross section of a typical mesh used in Flow-3D

4. Mathematical Modeling

Mathematical models have been developed to predict the particle transport and deformation on impact with a flat substrate during the HVOF combustion spraying of polymeric materials (Ref 11). The models of particle acceleration and heating in an HVOF jet are fully coupled and simultaneously integrated within the same FORTRAN code to predict particle velocity and temperature profiles at impact. A VoF (Ref 14) computational fluid mechanics package, Flow-3D, was used to predict splat shapes using results from the acceleration and heating models as initial conditions. A 2D slice of the computational domain including a fixed rectangular grid and a schematic representation of the initial and boundary conditions used here is shown in Fig. 3. The VoF method uses a fixed-grid volume tracking algorithm (Ref 14) to track the fluid deformation and droplet free surface based on a fluid fraction function, defined to be unity within the fluid and zero outside the fluid. The mesh resolution

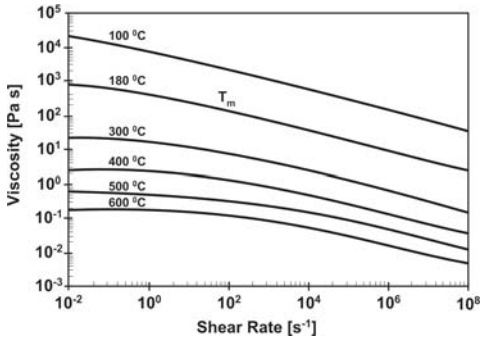

Fig. 4 Shear rate and temperature dependent viscosity of nylon 11 predicted using a Carreau model

was $D_{particle}/100$ for the lower third of the computational domain and $D_{particle}/50$ for the remainder of the computational domain, as illustrated in Fig. 3. More details of the mathematical models used to predict the particle transport and deformation on impact and to predict splat shapes presented have been reported elsewhere (Ref 11, 13).

As described previously, most of the polymer particles under HVOF conditions have higher temperatures at the surface than at the core. Consequently, during particle impact and spreading the local Reynolds number varies across the droplet owing to the temperature-dependent viscosity distribution. Moreover, when the particle begins deforming, the particle viscosity is also altered, based on the local fluid velocity (i.e., the local shear rate). Polymer viscosity during droplet spreading is therefore a function of both the temperature and shear rate. The viscous stress, including both shear thinning and temperature-dependent viscosity [$\mu(\dot{\gamma}, T)$], was modeled using a Carreau model (Ref 15). This model is included in the Flow-3D software in the form:

$$\mu = \mu_\infty + \frac{\mu_0 E_T - \mu_\infty}{\left[1 + (\lambda E_T)^2 \dot{\gamma}^2\right]^{[(1-n)/2]}} \quad \text{(Eq 1)}$$

The temperature dependence is given by:

$$E_T = \exp\left[a\left(\frac{T^*}{T-b} - c\right)\right] \quad \text{(Eq 2)}$$

where ($\mu_\infty = 0$) and ($\mu_0 = 13{,}000$ p) are the infinite shear-rate and zero shear-rate viscosities at a characteristic temperature ($T^* = 240$ °C), ($\lambda = 1$ s) is the time constant and ($n = 0.7$) a "power-law" exponent. All coefficients in the Carreau model including ($a = 16$), ($b = 0$), and ($c = 1$) were determined from experimental viscosity measurement performed by the authors. A plot showing the dependence of viscosity on both shear rate and temperature is shown in Fig. 4. In the model used, solidification, heat transfer from the splat to the substrate, and capillary effects, which were all previously shown (Ref 11, 13) to have secondary effects on the spreading of a molten polymer droplet, were neglected. Only conductive and convective heat transfer within the splats were evaluated.

Splatting of a 90 μm diameter nylon 11 droplet was predicted on both an ideally flat surface and on rough surfaces with three roughnesses expressed by R_a, R_q, and R_z:

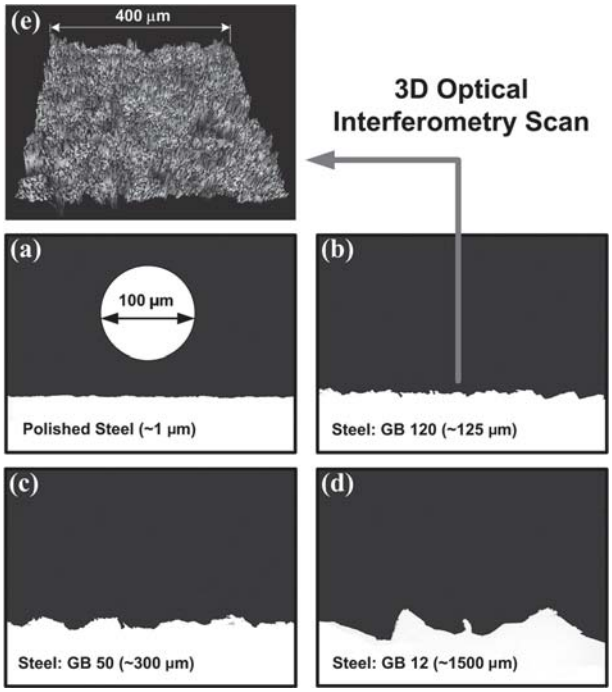

Fig. 5 Cross section of four steel substrates. (a) Polished with ~1 μm alumina suspension. (b) Grit blasted with No. 120 grit. (c) Grit blasted with No. 50 grit. (d) Grit blasted with No. 12 grit. Top image shows optical interferometric scan of No. 120 grit-blasted surface.

- Arithmetic average overall roughnesses (R_a) of 1.48, 2.96, and 5.92 μm
- Root mean square (rms) roughnesses (R_q) of 2.09, 4.18, and 8.36 μm
- Average maximum peak-to-valley heights (R_z) of 6.63, 13.25, and 26.5 μm

A roughened 3D surface was imported into Flow-3D from an optical interferometric scan of an actual grit-blasted steel surface (Fig. 5b and e) with an average roughness $R_a = 2.96$ μm, as typically used for thermally sprayed coatings. The resolution of the imported scans was 1 μm, which was compatible with the fine mesh resolution of the computation domain (Fig. 3). The grit-blasted surface was scanned using a Zygo Corp. (Middlefield, CT) *NewView 6000 3-D* optical profiling system. The roughness of the imported surface was also numerically scaled to generate two additional surfaces with average roughness of 1.48 and 5.92 μm for a parametric study.

5. Experiments

A semicrystalline polyamide 11 (nylon 11) powder commercially available as Rilsan PA-11 French Natural ES D-60 (donated by Arkema, Inc., King of Prussia, PA) was used as the feedstock material in this work. The as-received powder had a mean particle size of 60 μm and corresponding particle size distribution of (−120, +26 μm). The melting and degradation temperatures of nylon 11, as reported by the manufacturer, were in the range 182 to 191 °C and 357 to 557 °C, respectively.

Swipe or "splat" tests involving single high-speed (>0.7 m/s) spray passes across room-temperature steel substrates at low powder feed rates (~2 g/min) were used to observe the morphology of individual splats. The substrates used were 25 by 25 by 3 mm coupons of 4140 steel. The steel substrate was grit blasted using 125 μm (120 mesh), 300 μm (50 mesh), and 1500 μm (12 mesh) alumina grit at an angle of 45° with an air pressure of 0.55 MPa. The cross section of the grit-blasted substrates was prepared using standard metallographic techniques: sectioning, mounting and polishing, and analyzed by optical microscopy using an Olympus PMG-3 (Tokyo, Japan) optical metallograph.

Splat tests were carried out using a Jet-Kote II HVOF spray system (Stellite Coatings, Inc., Goshen, IN) using an O_2/H_2 ratio of 0.0024/0.0039 m^3/s (300/500 scfh) and a spray distance of 200 mm. Splat morphologies were analyzed using an FEI (Hillsboro, OR) XL-30 field-emission scanning electron microscope (SEM).

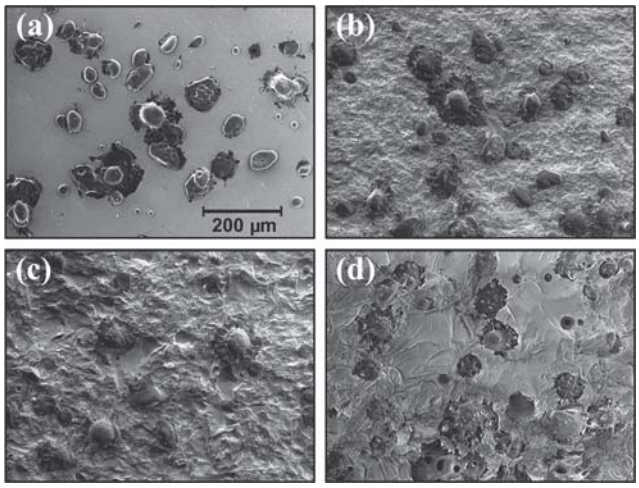

Fig. 6 Nylon 11 splats deposited during a single pass over steel substrates with roughnesses as per Fig. 5

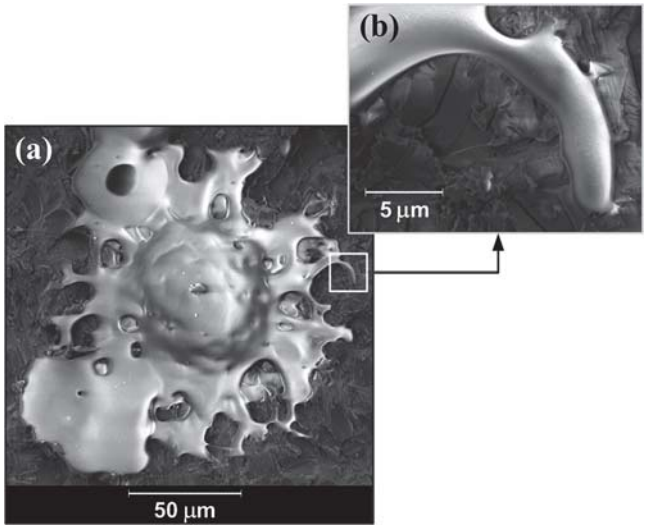

Fig. 7 Nylon 11 splat on a grit-blasted steel substrate. Enlarged view of a peripheral splat finger is shown in (a).

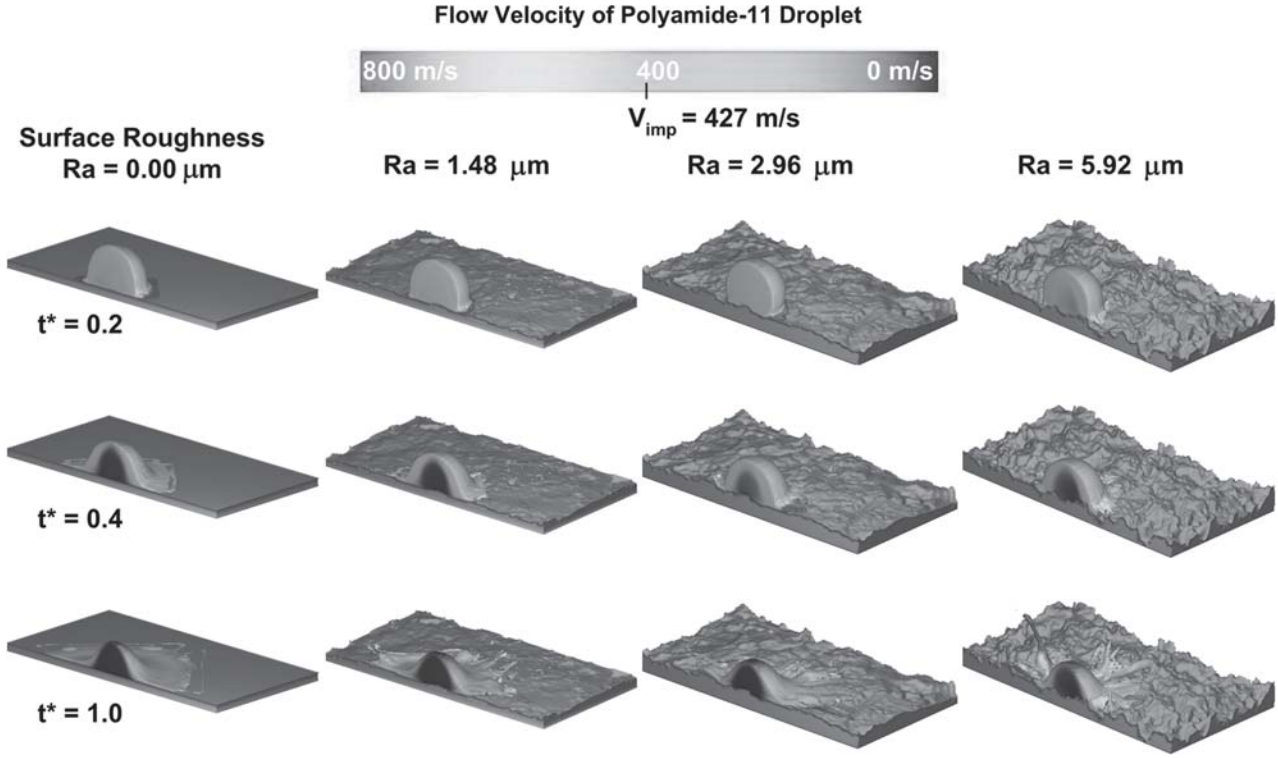

Fig. 8 Cross sections of predicted three-dimensional spreading splats for a 90 μm diameter nylon 11 particle on four different surface roughnesses (dimensionless time $t^* = t/(D_{initial}/V_{impact})$)

6. Results and Discussion

6.1 Experimental Results

The cross sections of one polished and three grit-blasted steel substrates used for the splat tests are shown in Fig. 5. The morphologies of nylon 11 splats deposited over these four surfaces during a single spray run are shown in Fig. 6. Most of the larger splats (>~100 μm) observed on all four substrates exhibited a characteristic "fried-egg" shape with a large, nearly hemispherical, core in the center of a thin disk. This observation was consistent with the previously reported (Ref 10) splat shapes deposited onto a flat glass slide substrate (Fig. 2b); however, a preliminary observation, after SEM analysis of the multiple splat regions, indicated that the final splat diameter decreased as the substrate roughness increased. Statistical analysis and quantification of this observation is currently in progress.

Preliminary observations also indicated that an increase in general substrate roughness promoted splat instability, resulting in radial jetting and breakup, and producing more irregularly shaped splat shapes on rougher surfaces (Fig. 6). This observation was consistent with the results published earlier by Fukanuma (Ref 6) and Syed et al. (Ref 16). Furthermore, it was observed that fingers on the periphery of the "fried egg" shaped splats solidified and settled on top of rough substrate asperities (Fig. 7b). This was believed to be caused by the high-speed radial flow and separation of the leading splat edge that spread over the top of the substrate asperities.

6.2 Modeling Predictions

Predicted 3D cross sections of spreading 90 μm diameter droplets on four different substrate surfaces are shown in Fig. 8. The droplets had an impact velocity of 427 m/s and internal temperature distribution, as shown in Fig. 1. The predictions exhibited a good qualitative agreement with the experimentally observed splats shown in Fig. 6 and 7. Larger splat spreading ratios ($D_{final}/D_{initial}$) occurred on smoother surfaces; that is, larger-diameter splats were predicted on an ideally flat surface (Fig. 8). Moreover, splat jetting/fingering was promoted as the substrate surface roughness increased, with the most prominent jetting occurring on the roughest surface, as indicated by the yellow and red splat fingers in Fig. 8 (R_a = 5.92 μm).

Cross sections of the predicted 3D 90 μm diameter splat revealed a fully conformed interface between the center of the splat and the underlying substrate topography (Fig. 9, detail A), while high-speed radial jets spread over the substrate asperities, (Fig. 9, detail B). This was believed to be caused by the high stagnation pressure below and around the center of the splat including a flow mainly directed normal to the surface, promoting filling of the surface cavities. On the other hand, after impact the droplet developed a "leading edge" with a relative velocity higher than the original impact velocity (Fig. 2a). The high velocity within the rim was the result of the squeezing flow between the relatively viscous particle core and the rigid substrate. This high shear rate flow led to low viscosity due to shear thinning, resulting in the very thin (2 to 5 μm) splat rim. The low viscosity and high shear rate in the rim and interaction with the substrate roughness contributed to the formation of jets and fingers. These predictions were in agreement with the experimentally observed radial finger morphology shown in Fig. 7.

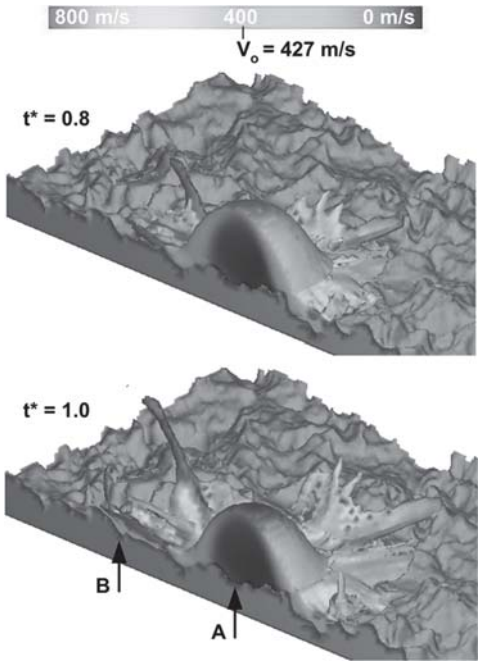

Fig. 9 Predicted three-dimensional spreading splats for a 90 μm diameter nylon 11 droplet

7. Summary and Conclusions

A particle splatting model and experimentally captured splats on nonsmooth surfaces have been studied to better understand how the geometric irregularities of a generally roughened surface affect the resulting polymer splat morphology. The morphology of the polymer splats initially thermally sprayed onto a substrate surface play a key role in the integrity of the coating/substrate interface and the overall adhesive strength of the coating. This is because the primary bonding mechanism of thermally sprayed coatings is often mechanical interlocking between the coating material and asperities on the roughened substrate.

Results, both experimental and numerical, indicated that an increase in the magnitude of the mean substrate roughness promoted splat instability (jetting and/or satellite breakup) and formation of radial fingers. It was also observed that an increase in general surface roughness may result in a lower spreading ratio ($D_{final}/D_{initial}$) of thermally sprayed polymer particles, which was consistent with observations made by other authors on metallic and ceramic splats.

The results also indicated that the center of a splat conformed well to the underlying substrate topography due to stagnation pressure and low shear rate flow directed steeply toward the surface encouraging the fluid to flow into surface cavities. On the other hand, the high-speed leading edge of a splat resulted from the squeezing flow between the viscous particle core and the rigid substrate. The low viscosity and high shear rate within the rim and interaction with the substrate roughness contributed to

the formation of radial jets and fingers, which flowed mainly parallel to the surface over the substrate asperities.

Statistical analysis of splat sizes on different general rough surfaces will be considered to quantify degree of spreading of polymer particles under different thermal spray conditions.

Acknowledgments

The authors would like to thank the National Science Foundation (NSF) for providing support for this research under collaborative grant number DMI 0209319. The views expressed in this paper do not necessarily reflect those of NSF. The authors would also like to thank Arkema Co. for donating the nylon 11 powder. The authors also greatly appreciate the assistance of Mr. Dustin Doss and Ms. Dee Breger. The assistance of Zygo Corp. with the surface roughness measurements reported here is also gratefully acknowledged.

References

1. J.R. Davis, et al., Ed., *Handbook of Thermal Spray Technology,* 1st ed., ASM International, 2004
2. P. Fauchais, M. Fukomoto, A. Vardelle, and M. Vardelle, Knowledge Concerning Splat Formation: An Invited Review, *J. Thermal Spray Technol.,* 2004, **13**(3), p 337-360
3. H. Liu, E.J. Lavernia, and R.H. Rangel, Modeling of Molten Droplet Impingement on a Non-flat Surface, *Acta Metall. Mater.,* 1995, **43**(5), p 2053-2072
4. V.V. Sobolev, J.M. Guilemany, and A.J. Martin, Influence of Surface Roughness on the Flattening of Powder Particles During Thermal Spraying, *J. Thermal Spray Technol.,* 1996, **5**(2), p 207-214
5. N.A. Patanker and Y. Chen, Numerical Simulation of Droplet Shapes on Rough Surfaces, *Proc. Fifth Int. Conference on Modeling and Simulations of Microsystems (MSM 2002)* (Puerto Rico), 2002, p 116-119
6. H. Fukanuma, Mathematical Modeling of Flattening Process on Rough Surfaces in Thermal Spray, *Thermal Spray: Practical Solutions for Engineering Problems,* Proc. Ninth National Thermal Spray Conf. (Cincinnati, OH), C.C. Berndt, Ed., ASM International, 1996, p 647-656
7. M. Raessi, J. Mostaghimi, and M. Bussmann, Droplet Impact During the Plasma Spray Coating Process—Effect of Surface Roughness on Splat Shapes, *Proc. 17th Int. Symposium on Plasma Chemistry* (ISPC 17) (Toronto, Canada), Int. Union of Pure and Applied Chemistry (IUPAC), 2005
8. M. Pasandideh-Fard, S. Chandra, and J. Mostaghimi, A Three-Dimensional Model of Droplet Impact and Solidification, *Int. J. Heat Mass Transfer,* 2002, **45,** p 2229-2242
9. Z.G. Feng, M. Domaszewski, G. Montavon, and C. Coddet, Finite Element Analysis of Effect of Substrate Surface Roughness on Liquid Droplet Impact and Flattening Process, *J. Thermal Spray Technology,* 2002, **11**(1), p 62-68
10. E. Petrovicova, "Structure and Properties of Polymer Nanocomposite Coatings Applied by the HVOF Process," Ph.D. dissertation, Drexel University, Philadelphia, PA, 1999
11. M. Ivosevic, R.A. Cairncross, and R. Knight, Impact Modeling of Thermally Sprayed Polymer Particles, *Proc. ITSC-2005 International Thermal Spray Conference* (Basel, Switzerland), DVS/IIW/ASM-TSS, 2005
12. Y. Bao, D.T. Gawne, and T. Zhang, The Effect of Feedstock Particle Size on the Heat transfer Rates and Properties of Thermally Sprayed Polymer Coatings, *Trans. I. M. F.,* 1998, **73**(4), p 119-124
13. M. Ivosevic, R.A. Cairncross, and R. Knight, "Heating and Impact Modeling of HVOF Sprayed Polymer Particles," *Proc. 2004 International Thermal Spray Conference (ITSC-2004)* (Osaka, Japan), DVS/IIW/ASM-TSS, 2004
14. C.W. Hirt and B.D. Nichols, Volume of Fluid (VoF) Method for the Dynamics of Free Boundaries, *J. Comput. Phys.,* 1981, **39,** p 201-225
15. B.R. Bird, R.C Armstrong, and O. Hassager, *Dynamics of Polymeric Liquids, Volume 1: Fluid Mechanics,* 2nd ed., John Wiley & Sons, 1987
16. A.A. Syed, A. Denoirjean, B. Hannoyer, P. Fauchais, P. Denoirjean, A.A. Khan, and J.C. Labbe, Influence of Substrate Surface Conditions on the Plasma Sprayed Ceramic and Metallic Particles Flattening, *Surf. Coat. Technol.,* 2005, **200,** p 2317-2331